Numerical Simulations of a Heavy Rainfall Case in South China

LOU Xiaofeng*[1,2] (楼小凤), HU Zhijin[2] (胡志晋), SHI Yuqin[2] (史月琴),
WANG Pengyun[2] (王鹏云), and ZHOU Xiuji[2] (周秀骥)

[1] *School of Physics, Peking University, Beijing* 100871

[2] *Chinese Academy of Meteorological Sciences, Beijing* 100081

(Received January 20, 2002; revised October 29, 2002)

ABSTRACT

Using a double-parameter non-hydrostatic elastic three-dimensional model with detailed microphysical processes, the authors simulate the heavy rainfall event in South China which occurred on 9 June 1998 and lasted for more than 3 hours. This case is a supercell, and the upward and downward drafts interact with each other, which transfers rich water vapor at the converging position to upper levels, and the two drafts together maintain the convective course. The vertical heating profiles and contributions to water matter of five kinds of micro-phase processes are revealed quantitatively in the results. Condensation releases the most heat, which is more than that of the absorption by evaporation and melting. The rain particles first come from the autoconversion of cloud particles, the warm-rain process; later from the cold-rain process, the melting of grauple particles. The precipitation intensity reaches 75 mm h^{-1} while its efficiency remains high. The total amount of rain is 32 mm, a value close to the observations of nearby stations.

Key words: non-hydrostatic atmospheric model, microphysics processes, rain mechanism

1. Introduction

Based on observation, strong convective clouds of heavy rainfall in China usually extend about 20–40 km, water vapor over a large range by stratiform clouds and the horizontal convergence of airflow that can extend one or two thousand kilometers result in their long duration. The model computational domain should be large enough to accommodate them, yet so much work has been done to simulate heavy rainfall with high-resolution meso-scale models, rather than cloud models. However, when horizontal grids are taken too small, for example 5 20 km, these models are no longer efficient since convection turns to grid-scale from the sub gridscale (Zhang et al., 1998). But explicit microphysics processes of many meso-scale models should be improved. For example, in the relatively detailed microphysics processes scheme of MM5, Reisner II or Goddard Graupel, some microphysical processes of ice-phased processes should be modified, such as sublimation of water vapor to cloud ice and the nucleation of cloud ice, etc. Meanwhile ice phase processes are important to precipitation (Ferrier et al., 1995). MM5 V3 has 8 explicit microphysical schemes (Lin et al., 1983; Reisner et al., 1998; Mccumber et al., 1991), in which only the Reisner II scheme predicts ice number content (N_i), and does not predict the number contents of rain (N_r), snow (N_s), graupel (N_g), and hail (N_h). As we know, if the number content is diagnosed, the truncated value (N_0) of particle spectra is constant. However in different rainfall cases, N_0, and particularly N_r, may vary rapidly. Sometimes the change of N_r in a case can reach two orders of magnitude. Thus if the model cannot well describe N_r and N_g which directly influence the precipitation forecast, this will limit the ability of the model to describe the features of spectra in different precipitation cases, and limit its ability to simulate and forecast rainfall.

Tao and Simpson (1989), Trier et al. (1996), and Shutt and Gray (1999) used meso-scale models developed from cloud models to simulate meso-scale convective systems of long time duration with the support of advanced computers, though in their schemes the N_0 for the size distributions is assumed to be constant. But in China the simulations of long time duration of convective systems are carried out very seldom to improve understanding of their microphysics processes and their feedback to dynamics, the precipitation mechanism, etc., especially for heavy rainstorms in South China. But these models cannot give very realistic initial fields because most of them trigger the model by using a homogeneous field and disturbance of

*E-mail: louxf@cams.cma.gov.cn

temperature and humidity, which limit the value of the model and affect its development. Nowadays the wind and temperature fields can be retrieved from Doppler radar data, which can be applied in the cloud model. Thus it avoids the start-up problem of the model using a non-homogeneous field. With the improvement of the simulating capacity of the meso-scale model, it is a good way to take the output of the meso-scale model with high resolution as the initial field of the cloud model. Yet such a strategy brings the difficulties of a non-homogeneous basic state. If we regard the horizontal mean value of the basic state as its true basic state, it is in accordance with the homogeneous basic state of the cloud model, though the disturbance includes part of it (Lou et al., 1998).

To delicately study microphysical processes of heavy rainfall, to analyze the contribution of different hydrometeors to precipitation and to study the impact of every microphysical process on precipitation and source of precipitation particles, it is important to use a nonhydrostatic model with explicit microphysics processes (Su et al., 1999) by explicit prediction of hydrometeor spectra in fully three-dimensional cloud models. To insure positive values and conservation of every hydrometeor, the model uses a time-splitting method, small time step size to calculate fast processes, and a non-negative advection method in space. And furthermore when one amount of hydrometeor is less than zero, another will make it up, which conserves the total mass.

This paper simulates heavy rainfall in South China using the three dimensional elastic meso-β model (Liu et al., 1993) which is developed from the cloud model of the two-parameter microphysics processes scheme of Hu Zhijin (Hu and He, 1988), where both mass contents and number concentrations of various water particles are predicted, and which analyzes convective development, microphysics characteristics, and the precipitation mechanism.

2. Case and model introduction

The sixth heavy rainfall event during Torrential Rainfall Experiment over both sides of the Taiwan Strait and adjacent area—HUAMEX, is from 8 June to 11 June 1998, when Guangdong and Fujian Provinces experienced a heavy rainfall. In Fujian, the rainfall centered in the north and central areas, and the maximum of this event was located in Pingtang City as 171 mm. The heavy rainfall was the result of a frontal trough, shear line, and southwest jet moving to Guangdong and Fujian Provinces under the unstable conditions before the westerly trough (Yi et al., 1998).

The sounding data on 0800 UTC 9 June 1998 at Fuzhou in South China was used in our model simulation. Figure 1 shows that the air was very humid, the vertical profile of temperature and its dewpoint were very close. The positive unstable energy is only 191 J kg^{-1}, the negative 39 J kg^{-1}, and the total 152 J kg^{-1}, a relatively stable stratification. North-south wind shear is not strong, and east-west shear averages 2 m s^{-1} km^{-1}, but peaks at 4 m s^{-1} km^{-1} at low levels. The convective cell moves east at about 11 m s^{-1}, and a moving coordinate is used to accommodate it within the simulated time (3 hours).

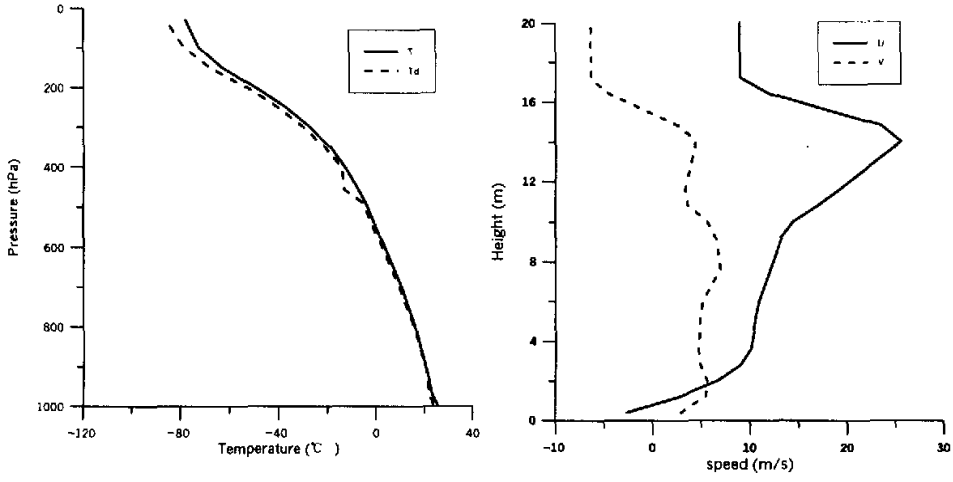

Fig. 1. Temperature and dewpoint (left), northern and eastern (right) wind components of the sounding data on 0800 UTC 9 June 1998 at Fuzhou.

The time-dependent, nonhydrostatic model used in this study is described in Hu (1988) and Liu et al. (1993). The predicted model variables are the potential temperature, pressure, the three velocity components, and the mixing ratios for water vapor and hydrometeors: cloud water (Q_v), rain water (Q_r), cloud ice (Q_i), graupel (Q_g), and hail (Q_h), and the latter four's numbers (N_i, N_r, N_g, N_h). Twenty-six kinds of microphysical processes are calculated, including condensation and evaporation (S_{vc}, S_{vr}), deposition (S_{vi}, S_{vg}, S_{vh}), collection (C_{cr}, C_{ci}, C_{cg}, C_{ch}, C_{ri}, C_{rg}, C_{rh}, C_{ir}, C_{ig}, C_{ih}, C_{ii}, C_{rr}), ice nucleation (P_{vi}), ice multiplication (P_{ci}), melting and freezing (M_{ir}, M_{gr}, M_{rg}, M_{hr}), and autoconversions of cloud to rain, ice to graupel and graupel to hail (A_{cr}, A_{ig}, A_{gh}). Cloud water and cloud ice are assumed to advect freely with the environmental airflow with negligible terminal velocities. The precipitation particles are heavier particles, although advected by the ambient wind, fall relative to the updraft with appreciable terminal velocities. The horizontal domain of the model is 120 km×120 km with a constant grid increment of 2 km. The top of the model is placed at 20 km, high enough to allow a supercell to develop. Boundary conditions are free-slip at the lower surface, rigid at the top, and open up-stream at the lateral boundaries.

3. Dynamic structure

A supercell is well captured by our model in this case. The continuous precipitation from 8 June caused such high humidity in the area that nearly all layers reached saturation. So we used a thermal disturbance of 1.5°C to initiate the model. The convective cloud developed fast after a while. The vertical velocity of this case was not very strong, and the peak vertical velocity was not more than 10 m s^{-1} during the 3-h simulation time. The updrafts increased quickly before rainfall occurred, peaking at 9 m s^{-1} at 100 min. Then the updrafts decreased a bit. The maximum value of 6 m s^{-1} held until the end of the simulation. While the intensity of updrafts increased, the updraft center rose to higher than the 10 km level at 60 min. The updrafts extended to about 15 km high and declined afterward. The horizontal domain of updrafts extended from 15 km at 20 min to 35 km at 200 min during the simulation, which is in accordance with the horizontal scale of the RHI (radar echo). The updraft center split into two parts that were maintained till the end of the simulation. Under the rear updrafts where precipitation appears occurred weak downdrafts that were less than 2 m s^{-1}. A cold high from the downdrafts coincided with the declined updrafts, which continuously transported sufficient water vapor of the convergence area to the high level. So in the high level there was enough water vapor over a long time to allow the hydrometeors to increase, which maintained the long convection. In Fig. 2, the time sequences of vertical velocity and $u - w$ streamlines are given. In order to better describe the airflow out of and into the cloud, the east-west direction wind component is modified so that strong winds are weakened and weak winds are strengthened, but the wind direction and the relative size among different levels are not changed. In the simulation, cloud moved to the right forward compared with the environment wind field, and formed an updraft and downdraft, which maintained convection of a long duration and improved cloud development. Updraft came from the right and climbed slantwise. Vertical velocity became bigger as altitude grew higher. It reached a maximum value in the medium-high level and then decreased. It was pulled out from the plume by high wind. Cold air from the rear cloud and downdraft caused by dragging of precipitation raindrops diffused in the ground layer, and partly moved downward of the updraft area. This is a classic structure of the supercell, and the simulated system was in a quasi-steady state for a long time. Though the coordinate system was moved eastward at 11 m s^{-1}, the cloud body shifted to the east lateral boundary after 200 simulated minutes, so the run was terminated.

To maintain a supercell for a long time, water vapor should be transported by updraft to the cloud continuously. In order to get a better understanding of this phenomenon, divergence and convergence of air flow and water vapor flux at 8 different height levels are listed in Fig. 3. During the 3-h simulation, both divergence and convergence of the lower levels were bigger than those of the middle levels and upper levels, which were caused by the rich water vapor of the lower levels of high temperature. In Fig. 3b, the water vapor flux presents convergence below 5.2 km, and from 7.6 km to 17.6 km height it takes on divergence, which peaks at 7.6 km. The values of convergence at different levels are much larger than that of divergence because a small part of convergent water vapor is transformed to liquid water or ice particles to form the cloud body, and most of it turns to the ground rainfall. The value of the convergence of water vapor flux is dominated by the water vapor at lower levels, so the small values of upper levels do not mean that the convergences or divergences are weaker than those of lower levels, which is testified by Fig. 3c. Obviously airflow also presents convergence at 0.4 km, 2.8 km and 5.2 km, and their curves are very close to each other. The other 5 levels over 5.2 km take on divergence and reach the maximum value at the 12.4 km level, near the location of the maximum vertical velocity. So the convergence of water vapor flux is bigger than its divergence. It shows convergence on the whole. Water vapor is continually transported from lower levels to high levels and flows out in high levels. In the 3-h simulation, a part of the

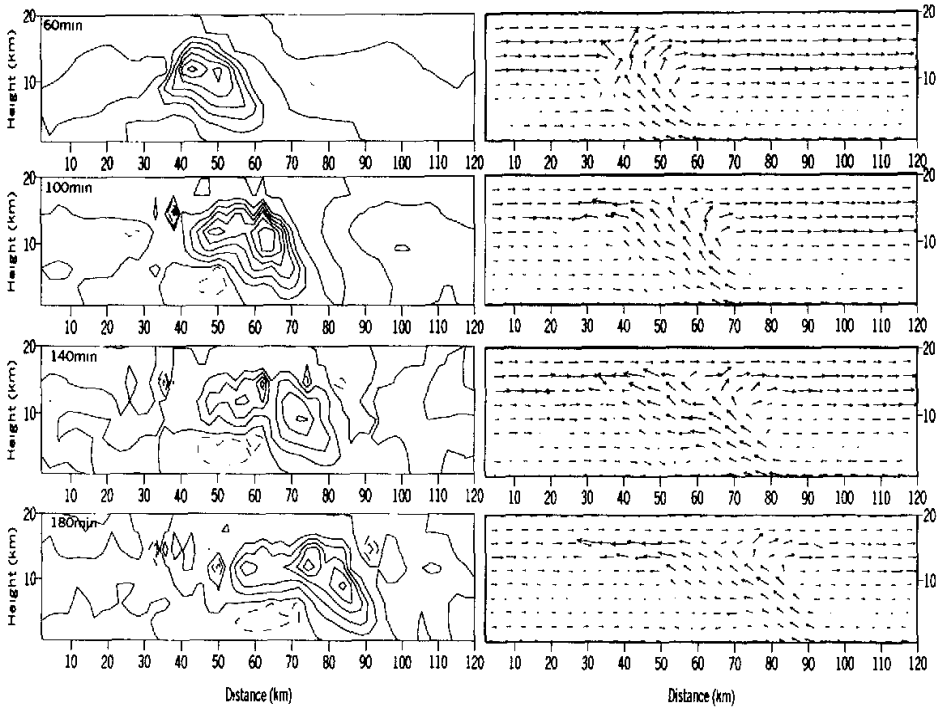

Fig. 2. Time sequences of $x-z$ sections of vertical velocity (left) and streamlines (right) at y=60 km, interval value is 1 m s^{-1}; solid lines stand for the updrafts, and dashed for downdrafts.

water vapor is converted to liquid or solid water all the time, which maintains development of convection and the duration of precipitation.

Simulated radar echoes and vertical distributions of the streamline field at four times are given in Fig. 4. The horizontal scale of the simulated echo extends continuously with the prolonging of the simulation, and slowly moves eastward, but the height of the echo does not change prominently. Because the radar echo is not mainly formed by ice crystals and cloud, but by raindrops and graupel, the strong echo area appears in the rear position of the strong updraft of the ground layer where plenty of raindrops and melting graupel can be found. The maximum echo intensity reaches 55 dBZ. Forward airflow takes away a part of the hydrometeors, which forms a sheet of plume of less than 15 dBZ. Doppler radar in Changle City of Fujian Province captured echoes within the simulation time. The data are not complete and do not fully match the simulation in time and space. But the magnitude of the simulated echo is in great accordance with the observed one, and the single echo is nearly reproduced.

4. Microphysics processes

MM5 is extensively used to simulate meso-scale weather process. It has a great advantage over cloud models in the aspect of dynamic fields, initial and boundary conditions, radiation and planetary boundary layer and so on. Whereas its microphysical process is weak though it includes 8 microphysical schemes, all of them were simplified from the cloud model. In MM5 the truncated value of the particle spectrum is constant, and for hydrometeors is diagnosed. But the truncated value of the raindrops, snow, and graupel (N_{or}, N_{os} and N_{og}) are different in different cases. Even in the same case they are different at different developing periods. If we regard them as constants, they do not coincide with reality. Autoconversion of particles is given a threshold that varies in different microphysical schemes, even in the same scheme of different versions of MM5. All of these things affect the simulation. If we use the simulation result of MM5 to analyze the microphysical process and precipitation mechanism, the result is not reasonable. But the number contents of particles are predicted in our double-parameter model. The process of cloud autoconversion to raindrops (A_{cr}) is defined by the predicted value spectrum width. Our model has a greater advantage than MM5 in the process of ice nuclei (P_{vi}), freezing of rain to graupel (M_{rg}), melting and sublimation of

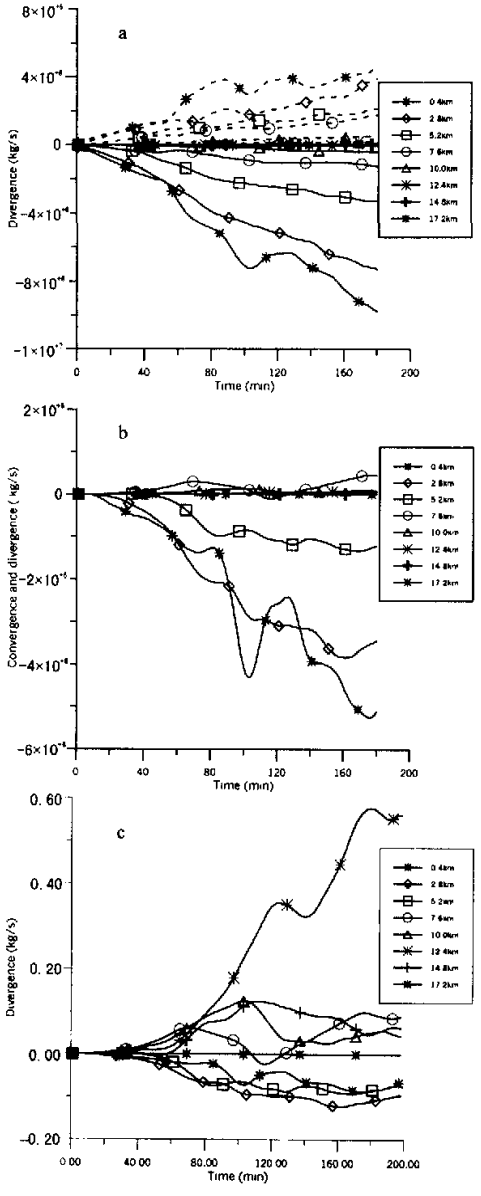

Fig. 3. Time variations of convergence and divergence of water vapor flux and air flow, a: convergence and divergence of water vapor flux at 8 levels, dashed presents divergence and solid means convergence; b: the sum of convergence and divergence of water vapor flux at the same 8 levels; c: divergence of air flow.

graupel (M_{gr} or S_{vr}), and so on. So the analysis of the microphysical process is meaningful, though the simulated convective process is developed from homogeneous initial conditions.

4.1 *Hydrometeors*

In this case, the cloud body extends to 18 km of height, and stretches horizontally for more than 70 km, which can be seen in Fig. 5. In order to better describe the airflow out of and into the cloud, the east-west directed wind is modified as in section 3. The upper part of the cloud is formed by cloud ice and graupel particles, and in the plume nearly by ice. Because of condensation caused by the upward movement of the air, the cloud water area coincides well with the updraft area, and splits into two centers with the splitting of updraft, and leans backward along with the slanting ascending air flow which is hung up over the downdraft area. There appear two cloud water centers at about 50 km and 70 km in horizontal distance. At the same time, because of near saturation, the bottom of the cloud reaches the ground. Graupel particles of 0.5 g kg^{-1} outline embrace most of the cloud water, cloud ice, and rainwater areas. Graupel is distributed extensively from 2 km to 17 km in height. It extends to the top of the updraft area, and its horizontal scope is about 50 km wide. Raindrops are distributed below 8 km high. Some of rain drops located around 60 km in horizontal distance can grow either from rain embryos of the autoconversion of cloud water or from melted graupel particles, through both the warm rain process and the cold rain process, but others located around 32 km× 35 km, where little cloud water exits, the rain particles can only be generated via the melting of graupel, which is a cold rain process.

4.2 *Phase transformation*

Microphysics processes include phase transformation and non-phase transformation processes. Latent heat is not released in the latter, but in the former water materials change from one phase to another phase among vapor, liquid water, and solid particles, and so latent heat is absorbed or released, which affects the air temperature and therefore affects the dynamic fields. Based on their initial phases and final phases, all phase transformation processes are divided into 5 categories: condensation, evaporation, sublimation, freezing, and melting.

Condensation: vapor to cloud water (positive S_{vc}); S_{vr} is very small, omitted;

Evaporation: cloud water to vapor (negative S_{vc}), rainwater to vapor (negative S_{vr});

Sublimation: vapor to ice (S_{vi}), vapor to graupel (S_{vg}), ice nucleation (P_{vi});

Freezing: cloud water collected by ice (C_{ci}), cloud water by graupel (C_{cg}), small raindrop by ice (C_{ri}) and

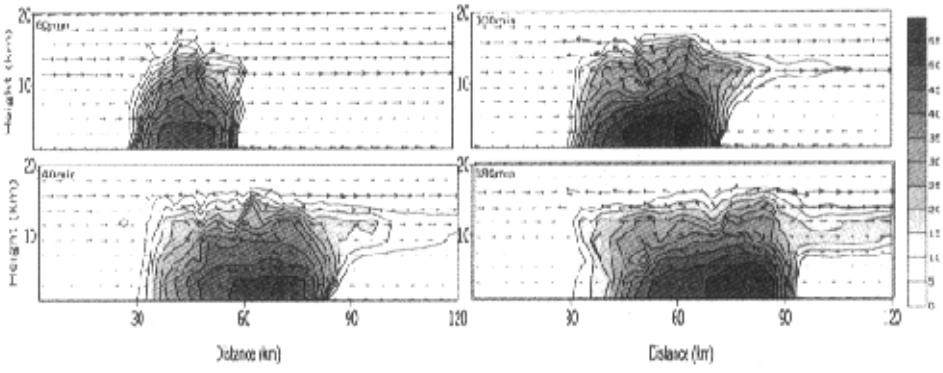

Fig. 4. Superimposed figures of streamlines and simulated radar echos, interval= 5 dBZ.

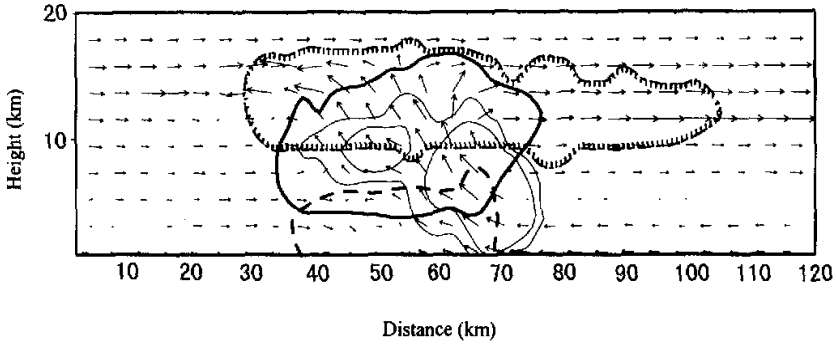

Fig. 5. Vertical section of hydrometeors (g kg^{-1}) described as a function of height at y=60 km, duplicated by the streamlines of u and w. The curves for the hydrometeors shown are cloud ice q_i (thin hatched, short dashed, contour of 0.1 g kg^{-1}), cloud water q_c (thin solid, contour of 0.1 g kg^{-1}), graupel q_g (thick solid, contour of 0.5 g kg^{-1}), rain q_r (thick long dashed, contour of 0.5 g kg^{-1}).

the multiplication of ice (P_{ci}), freezing of rain to graupel (M_{rg}), autoconversion of cloud to graupel (A_{cg});

Melting: ice collected by raindrop (C_{ir}), melting of ice (M_{ir}) and graupel (M_{gr}).

The amount of hourly hydrometeor mixing ratios and temperature caused by the 5 categories of phase transformation is described in Fig 6. Condensation begins nearly at the ground, extends to 12 km high, and the maximum value of 4 g kg^{-1} h^{-1} appears at 6 km high. Second to condensation, freezing and melting processes bring more than 2 g kg^{-1} s^{-1} of hydrometeors, peaking either above or below the zero temperature layer. Sublimation mainly exists at the plume where cloud ice contributes to solid particles, however from 4 km to 6 km of height the ice turns to water vapor via melting of solid particles. Evaporation is the least important process among the 5 categories.

Reliable information from direct measurements of latent heating released by deep cumulus clouds is not available. The cloud model can explicitly estimate feedback of phase transformation processes. Figure 6b shows the vertical distribution of the apparent heat source. Condensation releases the most relevant energy, which is larger than the absorption by melting and evaporation, and along with energy released by freezing and sublimation, the three provide energy for the convective system to develop. The cooling due to deposition and the warming due to melting occurred mainly near 5 km in height but above 7 km, sublimation displays positive feedback and peaks at 12 km. The cooling effect due to evaporation of raindrops mainly occurs below 4 km and a small number of cloud particles evaporate near 12 km high. Because of supercooled water, condensation appears at high levels

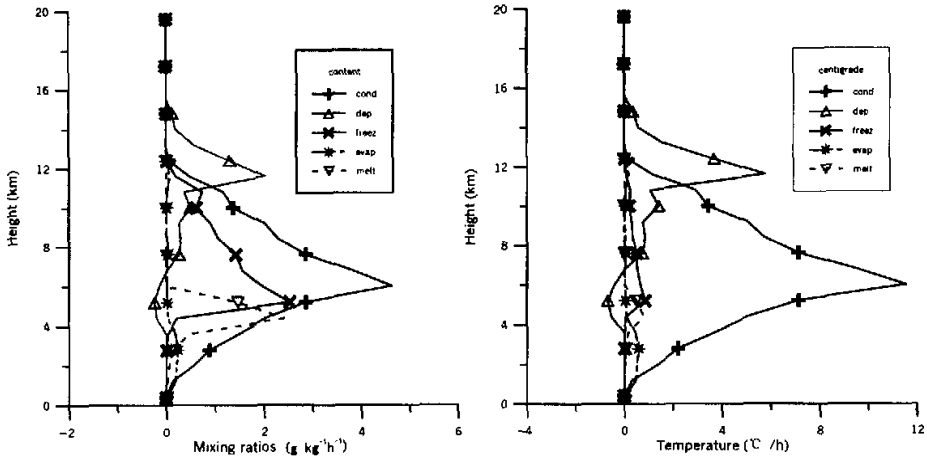

Fig. 6. Contributions to mixing ratios (left) and temperature (right) of 5 microphysics categories, these curves represent an average spanning the entire horizontal domain.

of the negative temperature area.

4.3 *Generation mechanisms*

The growth mechanism of particles and drops in hail clouds in stratiform clouds in South China are analyzed in detail for the purpose of hail suppression and rain enhancement. However, it is not well understood of heavy rainfall in some relatively rich rain areas, such as in South China. In this case, a large part of the clouds is warm. By which processes do precipitation particles grow? Which is much more important, warm rain process or cold rain process? In this section these issues are to be examined. To study the microphysical characteristics and precipitation mechanism of this case, we analyze the source and sink terms of cloud ice, graupel and raindrops, and particularly analyze the growth mechanism of raindrops. Equations of mass contents and their number concentrations of water vapor and five categories of water particles are described in section 2. Since hail particles are not important in this case, and the mass and number contents are negligible, processes related to hail are not considered.

The main out-growth courses of ice crystals are $P_{\rm vi}$ and $P_{\rm ci}$, and their main dissipation courses are $C_{\rm ir}$, $M_{\rm ir}$, $A_{\rm ig}$, and $C_{\rm ig}$. Ice mass transformation larger than 10^{-6} g kg^{-1} s^{-1} per grid point are four processes, as shown in Fig. 7a. Sublimation ($S_{\rm vi}$) contributes the most mass growth, though $P_{\rm vi}$ brings many ice embryos; the amount of mass is small because of the small mass of ice embryos. Auotconversion to graupel particles ($A_{\rm ig}$) and their collection ($C_{\rm ig}$) almost consume all ice particles mass contents. But the number mixing ratio of cloud ice increases mainly via ice nuclei ($P_{\rm vi}$) and ice multiplication ($P_{\rm ci}$) (shown in Fig. 7b). The former is mainly generated in the lower temperature area, and the latter is mainly generated in the upper temperature area, which only occupies one ten thousandth of the former. At the beginning ice droplets decrease via autoconversion to graupel embryos ($A_{\rm ig}$). After 40 minutes, ice droplets dissipate in turn via collection by graupel ($C_{\rm ig}$), autoconversion to graupel embryos ($A_{\rm ig}$), ice droplets melting to small raindrops ($M_{\rm ir}$), and collection by raindrops ($C_{\rm ir}$).

The change of mass contents of graupel mainly involves the 5 processes, $C_{\rm cg}$, $M_{\rm gr}$, $C_{\rm ig}$, $A_{\rm ig}$, and $S_{\rm vg}$ (shown in Fig. 7c). But only graupel melting to rain ($M_{\rm gr}$) expends some graupel mass. Graupel grows mainly by collection of cloud water ($C_{\rm cg}$). Collection of ice ($C_{\rm ig}$) and raindrops ($C_{\rm rg}$) contribute less to graupel. About 20 minutes after graupel embryos are generated by $A_{\rm ig}$, they grow via collection of cloud water and ice particles ($C_{\rm cg}$ and $C_{\rm ig}$). As for particle number (shown in Fig. 7d), $A_{\rm ig}$ first occurs at 20 min. and it nearly generates most of the graupel particles after 40 computational minutes. $A_{\rm cg}$, $C_{\rm ig}$, and $C_{\rm rg}$ generate a part of the graupel too. And some raindrops freeze to graupel.

At first raindrops grow via collection of cloud water ($C_{\rm cr}$), the warm rain process. Subsequently there appears the cold rain process (shown in Fig. 7e). That is to say that the value of melted graupel particles ($M_{\rm gr}$) increases quickly. It nearly reaches $C_{\rm cr}$ at 50 minutes and maintains its value till 180 minutes, which is to say that the warm rain process contributes the same to precipitation as the cold rain process. The main dissipation of rainwater is evaporation of raindrops ($S_{\rm vr}$)

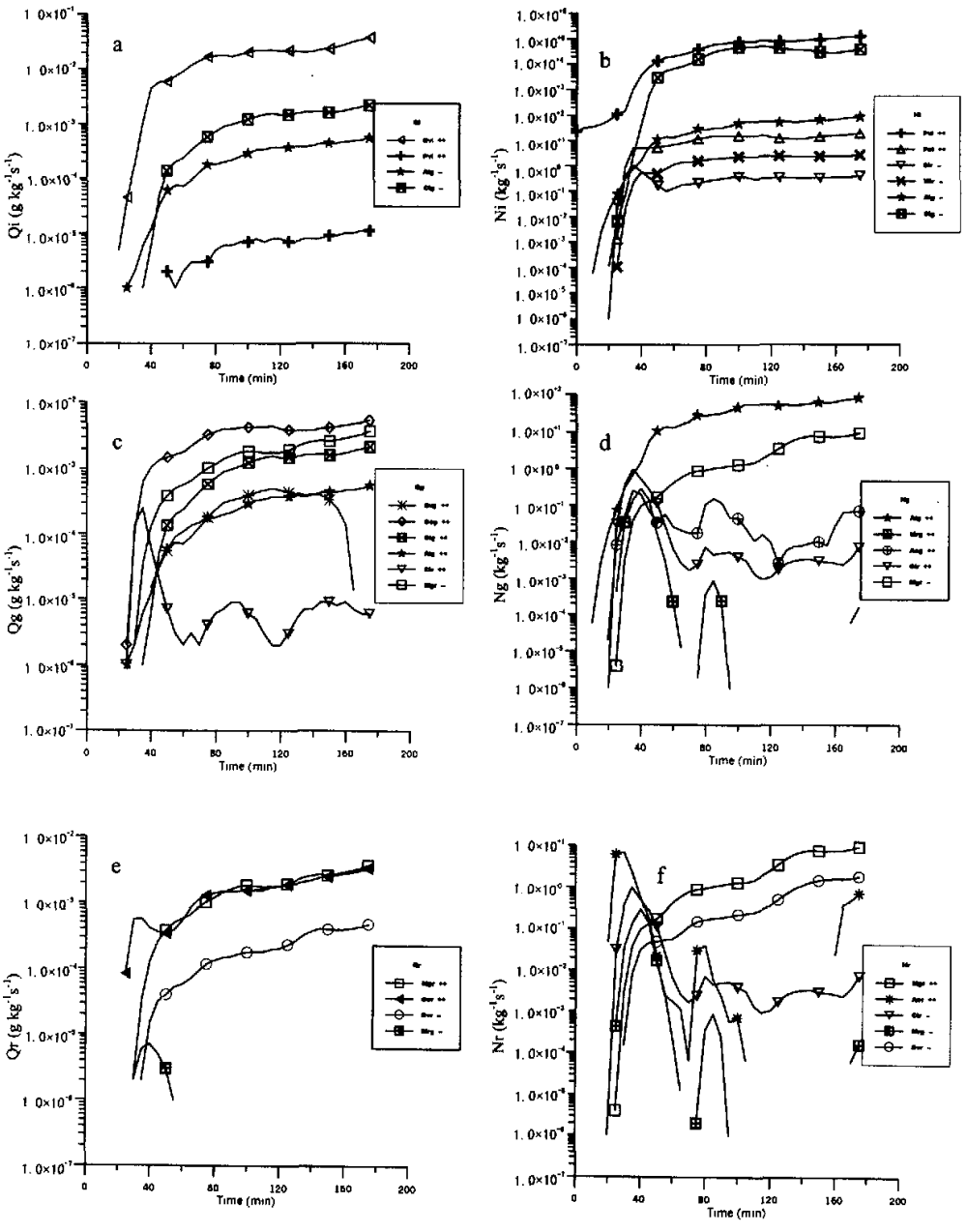

Fig. 7. Time variations of mixing ratios of mass and number content of cloud ice, graupel particles and rain drops, these curves represent an average spanning the 3D horizontal domain at every time step. a, c, and e are Q_i, Q_g and Q_r, respectively; b, d, and f are N_i, N_g and N_r, respectively.

except some raindrops frozen to graupel (M_{rg}) during the period 30 50 minutes. Because of the humid air, evaporation of rainwater (S_{vr}) is small. As for the number content of raindrops (shown in Fig. 7f), rain embryos appear via the warm rain process, which is autoconversion of cloud water (A_{cr}) at 20 minutes. They increase quickly from 0.1 kg^{-1} to 10 kg^{-1}, and then decline fast. But after 60 minutes raindrops again appear at 0.1 kg^{-1}. After 40 minutes melted graupel particles (M_{gr}) generate most raindrops, and the process becomes the main source of raindrops, which lasts till the end. The number content of raindrops decreases via evaporation of raindrops (S_{vr}), freezing of raindrops (M_{rg}), and collection by ice crystals (C_{ri}).

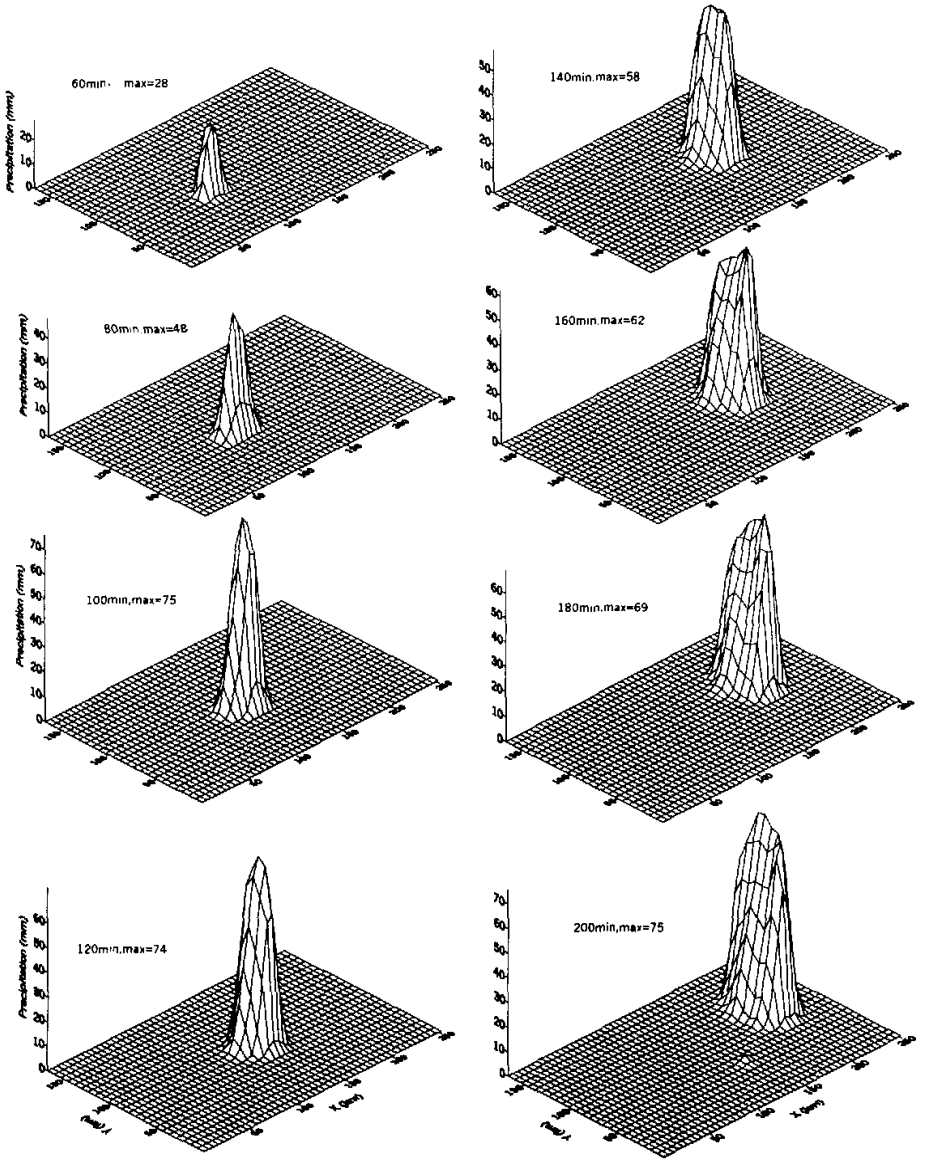

Fig. 8. Time sequences of precipitation intensity in ten-min average from 40 min to 200 min, the moving coordinate is considered to the domain, every vertical tick is 10 mm h^{-1}.

5. Simulated precipitation

The precipitation efficiency of this course reaches more than 30% during the period 40–200 minutes, and the intensity of precipitation grows steadily. Figure 8 shows the time sequence of the model-estimated rainfall rate over the horizontal domain. The simulated system moves a little relatively to the domain grid. At 40 min precipitation is very small, but at 60 min the intensity reaches 28 mm h^{-1}. The peak value reaches 75 mm h^{-1} at 100 min. Then the intensity declines slowly. But at 200 min the intensity reaches the peak value 75 mm h^{-1} again. During the whole simulation time, the position of the precipitation moves eastward gradually. Meanwhile the area of precipitation increase continuously and at 200 min it nearly reaches the northeast boundary of the simulated domain. To avoid the influence of the boundary, we end the simulation after 200 minutes.

The simulated accumulated rainfall is 32 mm, which is shown in Fig. 9. With convection moving eastward, the region of the rainfall extends eastward and the horizontal scale is larger than 100 km.

The observations show that from 8 to 9 June, some stations in Fujian Province experience rainfalls shifting between 25 mm and 90 mm. Lack of data at Fuzhou and Changle stations, we compare simulated precipitation with those of several neighbor stations. Around 1900 UTC, Minhou, Fuqing, and Minqing encountered heavy continuous rainfalls of 31 mm, 26 mm, and 22 mm respectively in four or five hours. So our model results in the 3-h simulation are comparable with observations though it is a little heavier than reality. It is regretful that our simulated horizontal domain is not large enough to lengthen the simulation, due to the limitation of computer memory.

6. Conclusions

Using an explicit double-parameter time-dependent, nonhydrostatic meso-β model with detailed microphysics processes, a heavy rainfall is simulated. The initial data, thermodynamic sounding data at 1600 UTC 9 June 1998, at Fuzhou City in South China is obtained from the HUMEX experiment. The horizontal domain of the model is 120 km×120 km with a constant grid increment of 2 km. The convective system moves east at about 11 m s^{-1}, and in order to keep it within the domain and away from the lateral boundary, a moving coordinate is used to accommodate it within the simulated time (3 hours).

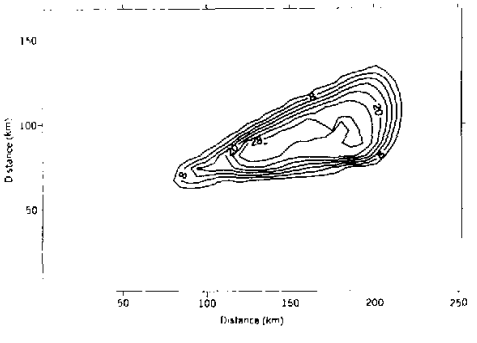

Fig. 9. The total rainfall in 3-h simulation, moving coordinate is considered to the domain.

The heavy rainfall from 8 June caused continuous precipitation in Fujian and Guangdong Provinces, which made the whole air saturated. We successfully triggered the model only using 1.5°C temperature perturbation. The vertical velocity of this case is not very strong, and the peak vertical velocity is not larger than 10 m s^{-1} during the 3-h simulation time. Downdraft coincides with declined updraft, which continuously transports sufficient water vapor in the convergence area to the high level. So in the high level there is enough water vapor over a long time to allow the hydrometeors to increase, which maintains the long convection. This is the classic structure of supercells. The analysis on the divergence of water vapor flux and the divergence of horizontal wind proves that water vapor converges in the low levels and diverges in the upper levels.

We analyze five phase transformation processes at all levels. Condensation brings the most mixing ratios of hydrometeors, and releases the most relevant energy, which is larger than the absorption energy by melting and evaporation. And along with the energy release by freezing and sublimation, it provides energy for the convective system to develop. To study the microphysical characteristics and precipitation mechanism of this case, we analyze the source and sink terms of cloud ice, graupel, and raindrops, and particularly analyze the growth mechanism of raindrops. Rain embryos appear via the warm rain process. At first raindrops grow via collection of cloud water (C_{cr}), the warm rain process. Subsequently there appears the cold rain process. That is to say that the value of melted graupel particles (M_{gr}) increases quickly. It nearly reaches C_{cr} at 50 minutes and maintains its value till 180 minutes, which is to say that the warm rain process contributes the same to precipitation as the cold rain process.

In this case the precipitation appears at 40 min and lasts till 200 min, the end of the simulation. The intensity reaches a quasi-steady state after 100 min of simulation time. The peak value of the precipitation intensity reaches 75 mm h^{-1} at 100 min during the 3-h simulation time. The precipitation efficiency of this course is bigger than 30%, and the simulated accumulated rainfall is 32 mm and extends about 100 km

within the 3-h simulation, somewhat close to the observed reality. In the future, we may simulate the case with periodic boundary conditions over a longer model time, such as 24 hours or even several days, to simulate the entire evolution of this rainfall process.

Acknowledgments. This work was supported jointly by National Key Basic Research Project G1998040912, 95 Special Topic of Key National Project: "Torrential Rainfall Experiment over the Both Side of the Taiwan Strait and Adjacent Area" (95-special-03) and the National Key Project of Science and Technology during the Tenth Five Year Plan 2001BA610A-06.

REFERENCES

Ferrier, B. S., W.-K. Tao, and J. Simpson, 1995: A double-moment multiple-phase four-class bulk ice scheme. Part II: Simulations of convective storms in different large-scale environments and comparisons with other bulk parameterizations. *J. Atmos. Sci.*, **52**, 249 280.

Hu Z. J., and He G. F., 1988: Numerical simulation of microphysical processes in cumulonimbus—Part I: Microphysical model. *Acta Meteorologica Sinica*, **2**, 471–484.

Lin Y.-L., R. D. Farley, and H. D. Orville, 1983: Bulk parameterization of the snow field in a cloud model. *Journal of Climate and Applied Meteorology*, **22**, 1065 1092.

Liu Y. B., Zhou X. J., and Hu Z. J., 1993: Three dimensional elastic nested-grid meso-($\beta - \gamma$) scale atmospheric numerical model. *Acta Meteorologica Sinica*, **51**, 369–380. (in Chinese)

Lou X. F., Hu Z. J., and You L. G., 1998: Test of non-hydrostatic model by using mesoscale non-homogeneous initial fields and simulation of front case. *Acta Meteorologica Sinica*, **56**, 55 67. (in Chinese)

Mccumber, M., W.-K. Tao, and J. Simpson, 1991: Comparison of ice-phase microphysical parameterization schemes using numerical simulations of tropical convection. *J. Appl. Meteor.*, **30**, 985–1004.

Reisner, J., R. M. Rasmussen, and R. T. Bruintjes, 1998: Explicit forecasting of supercooled liquid water in winter storms using the MM5 mesoscale model. *Quart. J. Roy. Meteor. Soc.*, **124**, 1071–1107.

Shutts, G. J., and M. B. Gray, 1999: Numerical simulation of convective equilibrium under prescribed forcing. *Quart. J. Roy. Meteor. Soc.*, **125**, 2767–2787.

Su H., Shuyi S. Chen, and C. S. Bretherton, 1999: Three-dimensional week-long simulations of TOGA COARE convective systems using the MM5 mesoscale model. *J. Atmos. Sci.*, **56**(14), 2326 2344.

Tao W.-K., and J. Simpson, 1989: Modeling study of a tropical squall-type convective line. *J. Atmos. Sci.*, **46**(2), 177-202.

Trier, S. B., W. C. Skamarock, M. A. Lemone, and D. B. Parsons, 1996: Structure and evolution of the 22 February 1993 TOGA COARE squall line: numerical simulations. *J. Atmos. Sci.*, **53**(20), 2861–2885.

Yi Q. J., Liu P., and Wang M. Z., 1998: The analysis of rainfall processes in 1998 during the HUAMEX experiment. *The Research of HUAMEX, 2000*, China Meteorological Press, Beijing, 4–12. (in Chinese)

Zhang, D.-L., 1998: The effects of diabatic physical processes on the simulations of mesoscale convective systems. *Chinese Journal of Atmospheric Sciences*, **22**(4), 435–451. (in Chinese)

一次华南暴雨降水过程的模拟分析

楼小凤 胡志晋 史月琴 王鹏云 周秀骥

摘 要

应用显式双参数微物理过程的β中尺度非静力平衡模式，利用福州市1998年6 月9日16时的加密探空资料进行了3小时的数值模拟。在模拟过程中形成的上升、下沉气流的有利配置，使得其前部的辐合区域丰富的水汽源源不断地往高层输送，从而维持了长时间降水，是一次超级单体过程。分析了五种相变过程的垂直分布情况及其对水成物和大气温度的贡献，凝结对这两者的贡献占最主要位置。在研究了降水粒子的比浓度和比质量的源汇项后，得出此次降水过程以暖雨过程开始，随后出现霰融化成雨滴并通过碰并云滴增长的冷雨过程。3小时的模拟降水范围超过了100 km，累积降水达到了32 mm，与附近站点的阶段降水实况比较接近。

关键词：非静力平衡模式，微物理过程，降水机制